

Gravitational scattering of solitonic boson stars: Analytics vs Numerics

Thibault Damour,^{1,*} Tamanna Jain,^{2,1,3,†} and Ulrich Sperhake.^{3,4,5,‡}

¹*Institut des Hautes Etudes Scientifiques, 91440 Bures-sur-Yvette, France*

²*LPENS, Département de physique, Ecole normale supérieure, Université PSL,
Sorbonne Université, Université Paris Cité, CNRS, 75005 Paris*

³*DAMTP, Centre for Mathematical Sciences, University of Cambridge, Wilberforce Road, Cambridge CB3 0WA, UK*

⁴*Department of Physics and Astronomy, Johns Hopkins University,
3400 North Charles Street, Baltimore, Maryland 21218, USA*

⁵*TAPIR 350-17, Caltech, 1200 E. California Boulevard, Pasadena, California 91125, USA*

(Dated: December 2, 2025)

We study the scattering of boson-star binaries, taking into account three effects: point-mass gravitational, tidal, and short-range scalar-field interactions. We compare analytic results to the scattering angle extracted from four sequences of numerical-relativity simulations at fixed energy and varying impact parameter. The very good agreement exhibits the attractive (repulsive) effect of in-phase (out-of-phase) binaries, which dominates at small impact parameters. We thus obtain the first effective-one-body potential, central for the construction of analytic gravitational-wave templates.

Introduction—The first direct detection of a gravitational wave (GW) signal, GW150914, from a black-hole (BH) binary [1], followed by $\mathcal{O}(100)$ further detections to date [2–5], has established gravitational-wave astronomy as a new pathway for exploring the physics of our universe. New tests of general relativity (GR) have added more evidence supporting the exceptional accuracy and range of validity of Einstein’s theory [6–8]. The multimessenger observation of the neutron-star (NS) binary system GW170817 [9] cemented a strong relation to short gamma ray bursts and efficient production of heavy elements.

While all events observed so far are compatible with compact binaries composed of NSs and BHs, the mass values inferred from some events raise intriguing questions. The analyses of GW190521 and GW231123 suggest constituent black holes (BHs) with masses $\gtrsim 85 M_\odot$ inside or above the pair-instability induced mass gap [2, 10], while the secondary of GW170814 with a mass $2.50 - 2.67 M_\odot$ would either be the heaviest NS or the lightest BH observed. These observations have naturally triggered investigations into the possibility of alternative, more exotic origins of these events as for example cosmic strings [11], Proca stars [12] or primordial black holes [13]. Furthermore injections of inspiral-merger-ringdown waveforms from boson stars (BSs) into simulated LIGO noise have revealed significant degeneracy between signals from BS and BH binaries [14]. Such exotic GW sources have attracted a lot of attention in diverse contexts as dark matter searches [15, 16], structure formation [17, 18], BH mimickers [19–22] or the validity of Thorne’s hoop conjecture [23].

Clearly, the capacity of GW observations to distinguish between BHs, NSs and exotic compact objects will be

crucial for identifying the nature of as yet unclassified sources, to understand their astrophysical origin, and to search for new physics beyond the standard model of particles. Systematic investigations are naturally drawn to two main characteristics of these diverse sources, (i) tidal interactions (e.g. [24]) and (ii) manifestations in either GW emission or the electromagnetic spectrum arising from the specific matter they are composed of (cf. [25] or the electromagnetic counter parts of GW170817).

In this work, we consider such effects (including the additional short-range scalar-field interaction) for the case of BS binary systems. A variety of stellar configurations composed of bosonic matter has been studied in the literature, as for example Proca stars [26] or ℓ BSs [27]. Here we focus on the class of BSs composed of a single complex scalar field first identified by Kaup [28]; see also [29], and Refs. [15, 30] for reviews. We treat BSs as electromagnetically dark, so that direct effects of their scalar matter will manifest themselves exclusively through overlap in the regime where the two BSs are in close vicinity. Tidal effects, on the other hand, will be present at any stage of the binary evolution, albeit with decreasing magnitude at larger distance.

In this work, we compute for BS binaries the effective potential central for the construction of analytic GW templates using the effective-one-body (EOB) formalism [31], which in itself uses results of various perturbative approaches: post-Newtonian (PN), post-Minkowskian (PM), Self-Force, Effective Field Theory (EFT) and Tutti Frutti. We furthermore employ numerical results which are necessary to determine the accuracy and validity of these approximants used to construct semi-analytic banks of waveform templates essential for detection and parameter estimation of GW events.

Whilst numerical relativity (NR) simulations of binary BSs have been performed for quasi-circular orbits, in this work we present the first simulations of binary BS scattering along with analytically deriving for the first time the effect of scalar interactions for binary BSs. We then

* damour@ihes.fr

† tj317@cam.ac.uk

‡ U.Sperhake@damtp.cam.ac.uk

compare the scattering angle χ determined from NR to the analytical estimates from an EOB-potential model including: point-particle results (BH), tidal effects and scalar field interactions. We find that the scalar effect dominates for small impact parameters while the tidal effects are sub-dominant; nonetheless, the inclusion of tidal effects order by order improves the agreement with NR data.

We use a “mostly plus” signature for the spacetime metric and employ units where the speed of light $c = 1$.

Theory— The action describing the dynamics of a complex scalar field φ minimally coupled to gravity is,

$$S = \int \frac{\sqrt{-g}}{2} \left\{ \frac{R}{8\pi G} - [g^{\mu\nu} \nabla_\mu \bar{\varphi} \nabla_\nu \varphi + V(|\varphi|)] \right\} d^4x, \quad (1)$$

where R is the Ricci scalar, g the determinant of the spacetime metric $g_{\mu\nu}$, an overbar denotes the complex conjugate and $V(|\varphi|)$ is the scalar-field potential. In this work, we consider solitonic potentials characterized by the scalar mass μ (with dimension of inverse length) and a parameter σ_0 ,

$$V(|\varphi|) = \mu^2 |\varphi|^2 (1 - 2|\varphi|^2/\sigma_0^2)^2. \quad (2)$$

Henceforth we use $\sqrt{G}\sigma_0 = 0.2$, which accommodates BS solutions with high compactness between that of NSs and BHs. The coupled Einstein-Klein-Gordon equations governing the BS solution are obtained by varying the action (1). Spherically symmetric solutions are obtained with the harmonic ansatz [32], $\varphi(t, r) = A(r)e^{i(\epsilon\omega t + \Phi)}$, where $A(r)$ is the (real) scalar field amplitude profile, ω is the frequency, and Φ is an initial phase. We also introduce a parameter $\epsilon = \pm 1$ determining the sense of rotation of the scalar field in the complex plane. By convention, $\epsilon = 1$ defines a BS while $\epsilon = -1$ is an *antiboson star* ($\overline{\text{BS}}$). Single BS and $\overline{\text{BS}}$ spacetimes are identical except for opposite Noether charge densities.

For a given value of the central scalar-field amplitude $A_{\text{ctr}} = A(0)$, the Einstein-Klein-Gordon equations along with boundary conditions for asymptotic flatness (typically) admit a unique ground-state BS (or $\overline{\text{BS}}$) solution. In this work, we consider $\sqrt{G}A_{\text{ctr}} = 0.17$ which corresponds to a BS containing 99% of its total mass m within a radius $r_{99} = 5.58 Gm$ ($= 3.98\mu^{-1}$).

Numerical Relativity (NR) Simulations— Our BS binary simulations have been performed using the LEAN code [33] based on the CACTUS COMPUTATIONAL TOOLKIT [34] using 4th-order finite differencing of the CCZ4 [35] version of the Einstein-Klein-Gordon equations. The code employs the moving puncture gauge and utilizes mesh refinement via CARPET [36]. Our computational domain extends to $448 GM$, where $M := m_1 + m_2 = 2m$ is the total BS rest mass, using 8 nested refinement levels with standard resolution $\Delta x = 0.02 GM$ on the innermost level. We employ outgoing Sommerfeld boundary conditions.

We study the scattering of two equal-mass ($\nu := m_1 m_2 / M^2 = 1/4$), nonspinning BSs with scalar fre-

TABLE I. Impact parameter b , total angular momentum J_{NR} , and the scattering angles (together with their error bars) for the four BS binary sequences as extracted from the numerical simulations. For all configurations, the total energy is $E/M = 1.02394$.

$\frac{b}{GM}$	$\frac{J_{\text{NR}}}{GM^2}$	$\chi_{\text{NR}}^{\text{BSBS}} [^\circ]$	$\chi_{\text{NR}}^{\text{BSBS}} [^\circ]$	$\chi_{\text{NR}}^{\text{BSBS}^{\frac{\pi}{2}}} [^\circ]$	$\chi_{\text{NR}}^{\text{BSBS}^\pi} [^\circ]$
9.9	1.15315	258.79(95)	216.41(1.41)	214.18(1.40)	198.41(1.26)
10.5	1.22360	170.51(89)	165.42(81)	165.28(81)	161.23(75)
11.0	1.28186	143.91(62)	142.32(60)	142.28(60)	140.83(58)
12.0	1.39839	114.43(64)	114.20(63)	114.33(53)	113.96(65)
13.0	1.51492	96.89(84)	96.89(84)	96.75(60)	96.81(82)
14.1	1.64982	83.39(1.14)	83.38(1.14)	83.32(1.10)	83.32(1.11)
15.0	1.74798	75.51(1.23)	75.73(1.37)	75.62(1.30)	75.62(1.30)
16.0	1.86450	68.16(1.27)	68.44(1.44)	67.97(1.14)	68.50(1.47)

quency $\omega = \omega_1 = \omega_2$. We investigate four distinct binary systems composed of a primary BS with fixed parameters ($\epsilon = 1$, $\Phi = 0$), and a secondary with parameters varying as follows: (i) ($\epsilon = 1$, $\Phi = 0$), denoted BSBS; (ii) ($\epsilon = 1$, $\Phi = \pi/2$), denoted BSBS $^{\frac{\pi}{2}}$; (iii) ($\epsilon = 1$, $\Phi = \pi$), denoted BSBS $^\pi$; and (iv) ($\epsilon = -1$, $\Phi = 0$), denoted $\overline{\text{BSBS}}$. The BSs start on the x -axis with initial positions $\pm X$ and initial velocity parameters $\vec{v} = (\mp v_x, \pm v_y, v_z)$, with corresponding kinematic momenta $\vec{p} := m\vec{v}/\sqrt{1 - \vec{v}^2}$. Unless specified otherwise, we set $|\vec{v}| = 0.2291$ and $X = 50.49 GM$. Defining the impact parameter $b := 2Xv_y/|\vec{v}| = 2Xp_y/|\vec{p}|$, the velocity vector of the two BSs is given by $(v_x, v_y, v_z) = \pm |\vec{v}|(-\sqrt{1 - (b/(2X))^2}, b/(2X), 0)$.

Initial data is constructed using the improved superposition of two boosted single-BS spacetimes as detailed in Ref. [37]. Residual constraint violations inherent to these data are further reduced by employing the CCZ4 formulation with constraint damping parameter $\kappa_1 = 0.1/M$ following Ref. [35]. We compute the binaries’ initial angular momentum from Eq. (17) below as $J = (1 + \epsilon_J)J_{\text{NR}}$, where J_{NR} is the Arnowitt-Deser-Misner (ADM) like integral (7.63) of Ref. [38] extrapolated to infinite extraction radius. The initial energy E is estimated as the sum of the relativistic (rest + kinetic) energy and the Newtonian binding energy including a parameter c_V for relativistic corrections,

$$E = 2 \frac{m}{\sqrt{1 - v^2}} - c_V \frac{Gm^2}{2X}; \quad (3)$$

see text below, and the Appendix A, for estimates of ϵ_J and c_V , and their justification.

We adopt a method similar to that of Refs. [39, 40] to determine the scattering angle. After converting the BS trajectories into standard polar coordinates (r, θ) and fitting the dependence of the angles on $1/r$ by polynomials $\theta_p := \sum_{n=0}^p \theta_n^p / r^n$, the angles (for each resolution) are obtained from the average $\bar{\theta} = (\theta_0^2 + \theta_0^3 + \theta_0^4 + \theta_0^5)/4$. As a conservative estimate of the error due to polynomial fitting, we use half the range of θ_0^p with $p = 1, \dots, 6$, yielding an uncertainty of 1.5° or less. A convergence analysis using additional resolutions $\Delta x = 0.022 GM$ and

0.017 GM and employing a fifth-order polynomial fit of the trajectory for the binary configuration $b = 9.9 GM$ yields second-order convergence with a discretization error $\sim 0.5^\circ$. Adding these two values in quadrature gives us a combined error budget $\Delta\chi_{\text{NR}} \sim 1.6^\circ$ or less. The results so obtained are displayed in Table I.

Analytical Relativity (AR) computation of χ —

Recently, there has been a significant effort on comparing analytic results to NR simulations of BH scattering [40–45]. Following Ref. [41], we analytically describe the scattering of BSs by transcribing the PM-expanded scattering angle $\chi(\gamma, j) = \sum_n 2\chi_n(\gamma)/j^n$ (where $j := J/(Gm_1m_2)$) into a corresponding energy-dependent EOB radial potential $w(\gamma, \bar{r}) = \sum_n w_n(\gamma)/\bar{r}^n$ (where $\bar{r} := \bar{R}/(GM)$ is a dimensionless isotropic EOB radial coordinate). Here, and in the following, γ denotes the EOB effective energy of the system, which is related to the total center-of-mass energy $E := Mh$ via $h = \sqrt{1 + 2\nu(\gamma - 1)}$ or, equivalently (for the equal-mass case $\nu = 1/4$), $\gamma = 2(E/M)^2 - 1$. [For scattering states, γ happens to be equal to the Lorentz factor between the two incoming world lines.] The dynamics of BS binaries involve two additional effects compared to those of BHs: tidal effects and scalar-field interactions, so that the PM-expansion of χ is naturally decomposed as

$$\chi(\gamma, j) = \chi^{\text{BH}}(\gamma, j) + \chi^{\text{tid}}(\gamma, j) + \chi^{\text{scalar}}(\gamma, j), \quad (4)$$

leading to a corresponding decomposition of the radial potential,

$$w(\gamma, \bar{r}) = w^{\text{BH}}(\gamma, \bar{r}) + w^{\text{tid}}(\gamma, \bar{r}) + w^{\text{scalar}}(\gamma, \bar{r}). \quad (5)$$

The PM expansion of w is uniquely determined by the PM expansion of χ via the EOB-derived map [46]

$$\pi + \chi(\gamma, j) = 2j \int_0^{\bar{u}_{\text{max}}(\gamma, j)} \frac{d\bar{u}}{\sqrt{p_\infty^2 + w(\bar{u}, \gamma) - j^2 \bar{u}^2}}, \quad (6)$$

where $\bar{u} = 1/\bar{r}$, $\bar{u}_{\text{max}} \equiv 1/\bar{r}_{\text{min}}$ and $p_\infty^2 = \gamma^2 - 1$.

Based on the 4PM knowledge of χ^{BH} [47], w^{BH} is fully known analytically up to 4PM order [41], and has been completed by a numerically fitted 5PM contribution, $w_5(\gamma)^{\text{BH, NR}}$ [42] – recall that w^{BH} is an effective potential that includes radiation-reaction effects¹. The tidal potential w_n^{tid} starts at 6PM, and is computed from the scattering angles derived in Refs. [47, 49, 50] using the following consequences of Eq. (6),

$$\chi_6^{\text{tid}} = \frac{15\pi}{32} p_\infty^4 w_6^{\text{tid}}, \quad \chi_7^{\text{tid}} = 4p_\infty^3 w_1 w_6^{\text{tid}} + \frac{8}{5} p_\infty^5 w_7^{\text{tid}}. \quad (7)$$

The last contribution to the potential, w^{scalar} , which describes the short-range scalar interaction between two BSs, has not been previously derived, nor its corresponding scattering-angle contribution part, χ^{scalar} . We have

computed the leading-order (LO) PM analytical value of w^{scalar} describing the conservative part of the scattering for BS binary, namely

$$w_{\text{LO}}^{\text{scalar}} = \frac{8\pi c_1 c_2}{Gm_1 m_2} \frac{e^{-\bar{m}\bar{r}}}{\bar{r}} \cos(\Phi_{21}). \quad (8)$$

Here, c_1 and c_2 are real scalar charges (defined in the next section), $\bar{m} \equiv GMh\tilde{\mu}$ [with $\tilde{\mu}^2 \equiv \mu^2 - (2\omega_1\omega_2\gamma - \omega_1^2 - \omega_2^2)/(\gamma^2 - 1)$] is an inverse range, and $\Phi_{21} := \Phi_2 - \Phi_1$ is the dephasing between the two interacting BSs' scalar fields. This corresponds to an attractive potential for BSBS ($\Phi_{21} = 0$), a repulsive one for BSBS $^\pi$ ($\Phi_{21} = \pi$), and a vanishing one for BSBS $^{\frac{\pi}{2}}$ ($\Phi_{21} = \pi/2$). For the BSBS case we obtain a fast-oscillating potential which averages to zero. These results confirm in a quantitative way the qualitative considerations of Appendix B of Ref. [51].

We sketch the derivation of our results as follows. Our starting point is an EFT action describing the two BSs (labelled by $A = 1, 2$) as worldlines $\mathbf{z}_A(\tau_A)$ endowed with time-dependent complex sources $s_A(\tau_A)$,

$$S_{\text{EFT}} = \int \frac{\sqrt{-g}}{2} \left\{ \frac{R(g)}{8\pi G} - [g^{\mu\nu} \nabla_\mu \bar{\varphi} \nabla_\nu \varphi + \mu^2 \bar{\varphi} \varphi] \right\} d^4x \\ - \sum_A \int \left\{ m_A - 2\pi [\varphi(\mathbf{z}_A) \bar{s}_A(\tau_A) + \bar{\varphi}(\mathbf{z}_A) s_A(\tau_A)] \right\} d\tau_A \\ + S_{\text{GF}}(g). \quad (9)$$

Here, $S_{\text{GF}}(g)$ fixes the harmonic gauge and τ_A is proper time. We keep only the quadratic term $\mu^2 \bar{\varphi} \varphi$ in the scalar potential because the higher-order terms $\sim \varphi^4 + \varphi^6$ lead to exponentially faster decaying interactions. The complex sources describing BSs are harmonically varying, i.e.

$$s_A(\tau_A) = c_A e^{i\epsilon_A \omega_A \tau_A + i\Phi_A}, \quad (10)$$

with constant (real) “scalar charges” c_A . The nonlocal character of s_A (via $\tau_A = \int^{z_A} \sqrt{-g_{\mu\nu}}(z'_A) dz'_A{}^\mu dz'_A{}^\nu$) can be described by using a Lagrange multiplier. The harmonically varying nature of the scalar sources $s_A(\tau_A)$ is a crucial new feature compared to existing EFT descriptions of point-like objects interacting in scalar-tensor theories of gravity.

The perturbative analysis from this EFT leads to Feynman-type diagrams computing the impulse $\Delta p_A^\nu := p_A^{\nu}{}_{\text{out}} - p_A^{\nu}{}_{\text{in}}$ of each body under the exchange of the scalar field together with gravity. The diagram Fig. 1a, describing scalar exchange between s_1 and s_2 , yields a LO contribution to the impulse of body one given by

$$\Delta p_{1\text{LO}}^\nu = -\frac{8\pi \tilde{\mu} c_1 c_2}{\sqrt{\gamma^2 - 1}} K_1(\tilde{\mu}|b|) \frac{b^\nu}{|b|} \cos(\Phi_{21}) \\ - \frac{8\pi c_1 c_2}{\sqrt{\gamma^2 - 1}} (\omega_1 \gamma - \omega_2) \tilde{u}_2^\mu \sin(\Phi_{21}) K_0(\tilde{\mu}|b|). \quad (11)$$

¹ However, the overall recoil has to be included separately [48].

Here, $\tilde{u}_2^\mu = (u_2^\mu - u_1^\mu \gamma)/(\gamma^2 - 1)$, $b^\nu = b_1^\nu - b_2^\nu$ is the impact parameter, K_1, K_0 are modified Bessel's functions, and $\tilde{\mu}$ is as above. The first (transverse) term on the right-hand side of (11) corresponds (using $j = p_\infty |b|/(GMh)$) to the scattering angle $\chi_{\text{LO}}^{\text{scalar}}$,

$$\frac{\chi_{\text{LO}}^{\text{scalar}}(j)}{h} = \frac{8\pi M \tilde{\mu}}{m_1 m_2} \frac{c_1 c_2}{\gamma^2 - 1} K_1(\tilde{\mu}|b|) \cos(\Phi_{21}) . \quad (12)$$

The second (longitudinal) term on the right-hand side of (11) predicts that the scattering is not conservative when $\Phi_2 \neq \Phi_1$. We have checked this prediction against NR data. This non conservative nature of the scattering can be analytically described by completing the conservative potential w^{scalar} by a dissipative force $\mathcal{F}_{\mu A}^{\text{scalar}}$ acting on each body. We checked on NR data, however, that the nonconservative nature of the scalar interaction introduces a negligible difference (for the cases we consider) between the scattering angle of particle 1, χ_1^{NR} , and that of particle 2, χ_2^{NR} , so that we can define $\chi^{\text{NR}} := \frac{1}{2}(\chi_1^{\text{NR}} + \chi_2^{\text{NR}})$. We henceforth discuss the construction of a scalar contribution, $w^{\text{scalar}}(\bar{r})$, in a radial potential (5) leading to χ^{NR} . Expanding Eq. (6) to linear order in w implies that the scalar contribution to χ is related to the scalar contribution to w via the following linear transformation

$$\chi^{\text{scalar}}(j) = -\frac{\partial}{\partial j} \int_{\bar{r}_{\min}}^{\infty} d\bar{r} \frac{w^{\text{scalar}}(\bar{r})}{\sqrt{p_\infty^2 - j^2/\bar{r}^2}} . \quad (13)$$

One readily checks that inserting in Eq. (13) the Yukawa-type potential $w_{\text{LO}}^{\text{scalar}}$, (8), gives rise to $\chi_{\text{LO}}^{\text{scalar}}$, (12).

To go beyond LO in the scattering angle, one needs to include both higher-order diagrams and iterated effects of the perturbed worldlines. The most relevant higher-order diagrams for our AR/NR comparison are 1b-1d which describe a $\mathcal{O}(G)$ gravitational dressing of Fig. 1a. Restricting ourselves to the equal-mass case, implying $c_1 = c_2$, $m_1 = m_2$ and $\omega_1 = \omega_2 = \omega$, we infer from matching the EFT results to the exact isolated, gravitationally dressed BS solution (see Eq. (19) below) that the leading fractional modifications of Eq. (12) for large impact parameter are logarithmic and of order $Gm_A((2\omega^2 - \mu^2)/\tilde{\mu}) \log(2e^{\gamma_E} \tilde{\mu}b)$. In the absence of exact results for the $\mathcal{O}(Gc_{ACB})$ contributions, we shall assume that the corresponding higher-order contribution to w can be approximated by the factorised form

$$w_{\text{HO}}^{\text{scalar}} = w_{\text{LO}}^{\text{scalar}} w_{\text{g-dressing}}^{\text{scalar}} , \quad (14)$$

with the following exponentiated gravitational dressing factor:

$$w_{\text{g-dressing}}^{\text{scalar}} = e^{GM((2\omega^2 - \mu^2)/\tilde{\mu}) \log(2e^{\gamma_E} GM \tilde{\mu} \bar{r})} . \quad (15)$$

We use the integral (6), with $w = w^{\text{BH}} + w^{\text{tid}} + w_{\text{HO}}^{\text{scalar}}$, to define the analytic prediction for the scattering angle.

Completing the AR description— The AR-predicted angle (4) depends on the knowledge of the following quantities: E (or equivalently $\gamma = 2(E/M)^2 - 1$),

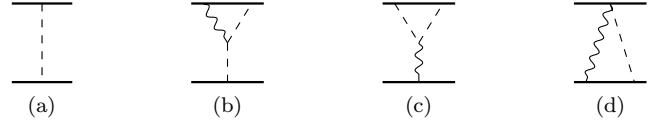


FIG. 1. Feynman diagrams needed for the computation of the scalar field effective action up to $\mathcal{O}(Gc_{ACB})$. The dashed (wavy) line represents the scalar (graviton) propagator.

J , w_5^{BH} , w_6^{tid} , w_7^{tid} , the scalar-charge parameters $c_1 (= c_2)$, and the phase difference Φ_{21} . We discuss their derivation in turn.

Residual constraint violations inherent to our initial data construction limit the accuracy of computing the initial values of E and J from their standard integral expressions. As discussed in the appendix A the approximate analytical expression (3) with $c_V = 1.37$, which yields,

$$\frac{E}{M} = 1.02394 \quad \text{with} \quad \gamma_{\text{in}} = 1.09690 , \quad (16)$$

defines a sufficiently accurate value of the initial energy; we adopt it in this work. In the absence of an analytic expression for J analogous to Eq. (3) (i.e. incorporating $\sim \frac{Gm}{2X} = \mathcal{O}(10^{-2})$ fractional corrections), we allow for a correction $J = (1 + \epsilon_J)J_{\text{NR}}$ to the ADM-like initial angular momenta listed in Table I, and determine best-fit values for ϵ_J in the following way. Since the scalar interactions average out for BSBS configurations their evolution most closely resembles BH scattering. We consequently use the subset of five BSBS simulations with $b/(GM) \leq 13.0$ together with analytic information about the scattering of BHs to fit $\epsilon_J = 0.006 \pm 0.001$ and, hence, use for *all* simulations

$$J = (1 + 0.006) J_{\text{NR}} . \quad (17)$$

Interpolating between the results of Refs. [39, 43], we have determined the effective 5PM contribution to the BH potential $w^{\text{BH}}(\bar{r}, \gamma)$ corresponding to our initial energy (16),

$$w_5^{\text{BH}} = -1.03 \pm 0.03 . \quad (18)$$

Next, we use the results of Ref. [52] to estimate the dimensionless even-parity quadrupolar tidal parameter $\Lambda_A := \lambda_A^{\text{tidal}}/(G^4 m_A^5)$, where λ_A^{tidal} denotes the tidal deformability of our solitonic BSs, and obtain $\Lambda_A \approx 7$ for each model. In the absence of corresponding results for the odd-parity quadrupolar and the even-parity octupolar tidal parameters, we insert $\Lambda_A \approx 7$ in Refs. [47, 49, 50] to determine χ_6^{tid} and χ_7^{tid} and then use Eq. (7) to obtain the corresponding tidal coefficients w_6^{tid} , and w_7^{tid} entering the EOB w -potential.

The scalar charges c_A are determined by matching the (gravitationally dressed) EFT-predicted analytic expression of the asymptotic scalar profile generated by an

isolated BS in harmonic coordinates, namely (recalling $\bar{\mu}_A := \sqrt{\mu^2 - \omega_A^2}$),

$$A(r) \approx \frac{c_A}{r} \exp \left[-\bar{\mu}_A r + Gm_A \frac{2\omega_A^2 - \mu^2}{\bar{\mu}_A} \log(2e^{\gamma_E} \bar{\mu}_A r) \right]. \quad (19)$$

to the scalar profile numerically computed for isolated BSs. For our models with $G\mu m_A = 0.713$ and $\omega_A = 0.439\mu$ we obtain $\sqrt{G}\mu c_A = 1.608$.

Comparison between AR and NR results— We now compare our AR predictions χ_{AR} , defined by Eq.(6), with our full set of 32 NR scattering data χ_{NR} (see Table I) composed of four types of BS binaries, each simulated for eight values of J (or, equivalently, b).

Fig. 2 presents a global view of the comparison between our AR predictions (solid lines) and the corresponding NR data (circles). For all four sequences, the agreement is visually excellent for most impact parameters, and exhibits a small worsening only for the smallest impact parameters (leading to very large scattering angles, $\chi > 200^\circ$). Our AR predictions are presented both in their full version (using $w = w^{\text{BH}} + w^{\text{tid}} + w^{\text{scalar}}$) and a version using $w = w^{\text{BH}} + w^{\text{HO}}$.

We quantify the (percent level) AR-NR agreement by displaying in Fig. 3 the fractional differences $(\chi_{\text{AR}} - \chi_{\text{NR}})/\chi_{\text{NR}}$. Further details about the NR/AR comparison are given in Table II, which explores the effect of various versions of the radial potential such as including only LO scalar interactions and/or various tidal terms. There, we define the quantity $\delta_\chi := (\chi_{\text{AR}} - \chi_{\text{NR}})/\Delta\chi_{\text{NR}}$ that measures the deviation of AR from NR values in units of the NR error estimate $\Delta\chi_{\text{NR}}$. Note that δ_χ is of order unity for our most accurate AR models.

The use of an analytic description based on w^{EOB} -resummed angles is crucial to reach this level of agreement; PM-expanded angles would exhibit up to an order of magnitude larger differences from NR data for nearly all impact parameters. The best agreement is obtained for the BSBS sequence (black lines in Fig. 2) which, as expected, is very close to BH-binary scattering; that agreement was obtained by fitting only one parameter, namely ϵ_J . As indicated, tidal effects are small even for small impact parameters, $b = 9.90M, 10.5M$. The agreement for the BSBS $^{\frac{\pi}{2}}$ sequence (green symbols in Fig. 2) is nearly as good, and also close to the BBH case. Its slightly larger disagreement for small b (leftmost data points in Fig. 3) likely arises because the vanishing of the w potential for BSBS $^{\frac{\pi}{2}}$ is only valid at LO, i.e. only for the diagram Fig. 1a. Excellent agreement with NR data is also obtained for the other two configurations, (i) BSBS (blue), and (ii) BSBS $^\pi$ (red). These cases also clearly demonstrate the attractive (repulsive) character of the scalar-mediated potential w^{scalar} , when $\Phi_{21} = 0$ ($\Phi_{21} = \pi$). In the attractive BSBS case, the two stars get very close to each other, $\bar{r}_{\text{min}} \approx 6.8$, and $w_{\text{HO}}^{\text{scalar}}$, Eq. (14), becomes quite significant; cf. Table II.

Our results also display the sub-dominant effect due to electric-type, quadrupolar tidal interactions. The in-

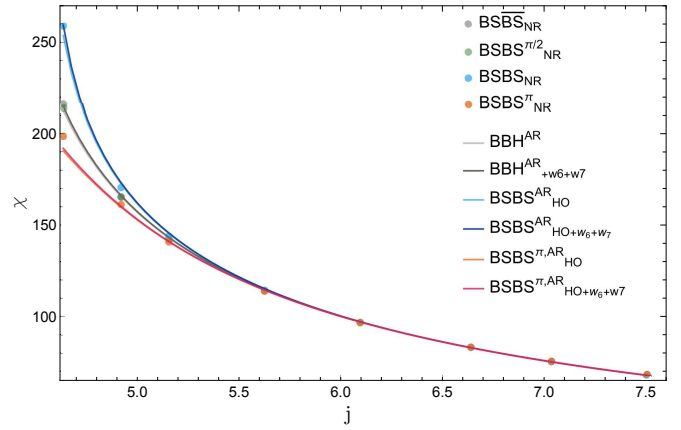


FIG. 2. Scattering angle comparison between the NR data (filled circles) and the EOB-resummed, PM based analytical prediction (AR; solid lines) for equal-mass, non-spinning boson star configurations for various rescaled initial angular momentum ($j = J/(Gm_1 m_2)$).

clusion, order by order, of the tidal potentials w_6^{tid} , w_7^{tid} , while nearly negligible for medium and large b , improves the agreement with NR data for all configurations with small impact parameters Appendix B.

Conclusions— We have performed the first numerical computation of the scattering angle χ of nonspinning, equal-mass BS binary encounters with scattering angles between 68.2° and 259° . Our key results include: (i) the derivation of the analytical LO scalar-exchange contribution to the scattering based on the EFT action (9) involving harmonically-varying scalar sources, (ii) inclusion of the gravitational-dressing effects to complete the LO scalar interactions with HO effects, and (iii) determination of the effective scalar charges c_A by matching to NR computations of isolated BSs to EFT predictions.

The comparison of the numerical/analytical results for BSs shows (i) the dominant effect due to scalar interactions, and (ii) the subdominant but real effect due to tidal interactions when the two stars get close. This indicates that the nature of the constituent matter of *exotic* compact objects can contribute more significantly to the dynamics than the tidal interactions.

Our simulations also revealed that for small impact parameters both BSs collapse into BHs after their close encounter and before separating to infinity. This phenomenon was not observed in quasi-circular BS binaries with the same compactness, highlighting the potentially important role of time-dependent scalar perturbations in destabilizing BSs and triggering collapse. This opens a novel direction for probing smoking gun-signatures of exotic compact objects.

ACKNOWLEDGMENTS

T. D. and T. J. thank Romain Gervalle for confirming the scalar charge of boson-stars. T. J. is

TABLE II. Summary of the AR scattering angle for various EOB predictions with impact parameter b . Here, $\delta_\chi = (\chi_{\text{AR}} - \chi_{\text{NR}})/\Delta\chi_{\text{NR}}$ measures the deviation of AR from NR values in units of the NR error estimate.

$\frac{b}{GM}$	BBH χ_{AR} [°]	$\delta_\chi^{\text{BSBS}}$	$\delta_\chi^{\frac{\pi}{2}}$	$\chi_{\text{LO,AR}}^{\text{scalar}}$ [°]				$\chi_{\text{HO,AR}}^{\text{scalar}}$ [°]				$\chi_{\text{HO},w_6,\text{AR}}^{\text{scalar}}$ [°]				$\chi_{\text{HO},w_6+w_7,\text{AR}}^{\text{scalar}}$ [°]			
				BSBS	δ_χ	BSBS $^\pi$	δ_χ^π	BSBS	δ_χ	BSBS $^\pi$	δ_χ^π	BSBS	δ_χ	BSBS $^\pi$	δ_χ^π	BSBS	δ_χ	BSBS $^\pi$	δ_χ^π
9.9	212.44	-2.81	-1.24	-	-	110.41	-69.84	253.68	-5.38	190.44	-6.33	256.24	-2.69	191.12	-5.79	259.32	0.56	191.89	-5.20
10.5	165.62	0.25	0.42	-	-	115.45	-61.04	172.51	2.25	159.78	-1.94	172.83	2.61	160.01	-1.63	173.11	2.93	160.21	-1.36
11.0	143.10	1.30	1.36	371.98	367.86	115.60	-43.50	145.47	2.50	140.90	0.12	145.58	2.69	141.00	0.30	145.67	2.84	141.09	0.45
12.0	114.90	0.12	1.08	124.70	16.06	107.50	-9.93	115.27	1.32	114.53	0.90	115.31	1.37	114.56	0.93	115.32	1.40	114.58	0.96
13.0	97.21	0.38	0.76	99.16	2.70	95.39	-1.73	97.28	0.46	97.14	0.40	97.29	0.47	97.15	0.42	97.30	0.48	97.15	0.42
14.1	83.12	-0.23	-0.19	83.46	0.07	82.76	-0.50	83.12	-0.23	83.10	-0.20	83.12	-0.23	83.10	-0.20	83.13	-0.23	83.10	-0.20
15.0	75.39	-0.24	-0.18	75.50	-0.01	75.28	-0.27	75.39	-0.10	75.39	-0.18	75.40	-0.10	75.39	-0.18	75.40	-0.10	75.39	-0.18
16.0	68.03	-0.28	-0.05	68.06	-0.08	68.01	-0.34	68.03	-0.10	68.03	-0.32	68.03	-0.10	68.03	-0.32	68.04	-0.10	68.03	-0.32

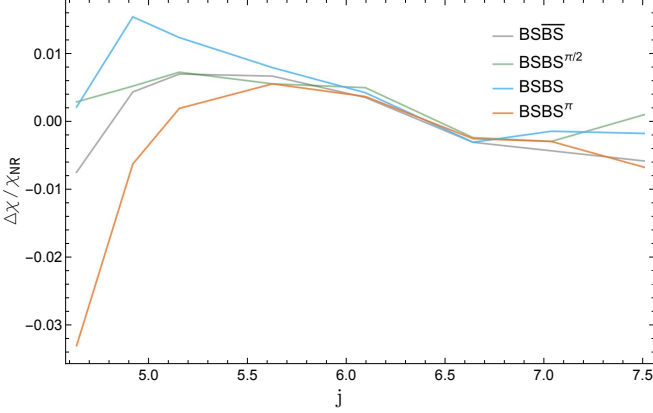


FIG. 3. Fractional differences $\Delta\chi/\chi_{\text{NR}} = (\chi_{\text{AR}} - \chi_{\text{NR}})/\chi_{\text{NR}}$ of analytical results (including both the tidal and scalar interactions) with respect to the numerical results.

supported by a LabEx Junior Research Chair Fellowship at ENS, Paris. T. J. thank the hospitality and the stimulating environment of the Institut des Hautes Etudes Scientifiques (IHES). The present research was partially supported by the 2021 Balzan Prize for Gravitation: Physical and Astrophysical Aspects, awarded to T. Damour. This work has been supported by STFC Research Grant No. ST/V005669/1. We acknowledge support by the NSF Grant Nos. PHY-090003, PHY-1626190 and PHY-2110594, DiRAC projects ACTP284 and ACTP238, STFC capital Grants Nos. ST/P002307/1, ST/R002452/1, ST/I006285/1 and ST/V005618/1, STFC operations Grant No. ST/R00689X/1. Computations were done on the CSD3 and Fawcett (Cambridge), Cosma (Durham), Stampede2 (TACC) and Expanse (SDSC) clusters.

Appendix A: Calculation of Initial Energy

There are two features of our numerical setup that *a priori* affect the accuracy of our analytical results: (i) the non-Cartesian value of the asymptotic spatial metric $\gamma_{ij}^\infty \neq \delta_{ij}$; and (ii) constraint violations in the initial data.

The feature (i) has a nearly negligible effect on our results for the following reason. The asymptotic spa-

tial metric of the improved superposition of two boosted single-BS spacetimes with BS distance r_{AB} is $\gamma_{ij}^\infty = 2\delta_{ij} - \gamma_{ij}^B(x_A^i)$; cf. Eqs. (45) in [37]. To a good approximation this is $\gamma_{ij}^\infty \approx (1 - 2Gm/r_{AB})\delta_{ij}$, which differs from a Cartesian metric by a factor $a^2 = 1 - 2Gm/r_{AB} = 1 - GM/r_{AB}$. Such a factor in the asymptotic metric can be reabsorbed in a common rescaling of the units of length, time and mass by a factor a (this leaves G and c fixed). Such a rescaling changes, for instance, the numerical value of the ADM mass-energy (with respect to using the usual Cartesian-based integral expression of the ADM energy) as $E_{\text{ADM}}^{\gamma_{ij}^\infty} = E_{\text{ADM}}^{\delta_{ij}}/a$, which, for our initial data ($a^2 \approx 1 - 1\%$), means an increase of E_{ADM} by about $+0.5\%$. However, this common rescaling of units of length, time and mass leaves invariant all dimensionless quantities (such as E/M , $J/(GM^2)$ and χ) and therefore can be ignored when comparing the function $\chi^{\text{AR}}(E/M, J/(GM^2))$ to χ^{NR} ; cf. Sec. 3.1 of [53] for a similar discussion of the irrelevance of the Doppler effect in binary pulsar gravitational tests.

The second feature (constraint violations) impacts the ADM-like evaluation of E from the initial time slice ($t = 0$) without affecting the BS masses. It thereby affects the numerical value of the dimensionless ratio E/M , which plays a crucial role in our AR/NR comparison. When ignoring the rescaling factor linked to $\gamma_{ij}^\infty \neq \delta_{ij}$, i.e. when computing the ADM-like initial energy (at $t = 0$) by using Eq. (7.15) of Ref. [38] (which assumes $\gamma_{ij}^\infty = \delta_{ij}$) one obtains (exactly) the sum of the ADM integrals for two boosted Schwarzschild metrics,

$$E_{\text{ADM}}^{\text{NR}}(t=0) = E_{\text{kin}}(v) = 1.027324M. \quad (\text{A.1})$$

Here the numerical value is obtained by inserting $v = 0.2291$ into the special-relativistic expression for the kinetic energy E_{kin} of two moving bodies,

$$E_{\text{kin}} := \frac{m_A}{\sqrt{1-v_A^2}} + \frac{m_B}{\sqrt{1-v_B^2}} = \frac{2m}{\sqrt{1-v^2}}. \quad (\text{A.2})$$

Extrapolating our numerical evaluation of the ADM integral to infinite radius yields $E_{\text{ADM}}^{\text{NR}}(t=0) = (1.027095 \pm 0.000361)M$ compatible with Eq. (A.1).

The value (A.1), however, represents only the kinetic energy of two moving bodies and does not account for the

system's gravitational binding energy. A more accurate value of the total incoming energy of the system differs from the kinetic-energy (A.2), by an additional term approximately equal to the Newtonian potential energy,

$$V_N = -\frac{Gm_A m_B}{r_{AB}} = -\frac{Gm^2}{2X} \approx -0.002476M. \quad (\text{A.3})$$

We indeed obtain such a correction by taking into account the effect of the initial violations in the Hamiltonian constraint which we write as

$$\mathcal{H}_0 := \mathcal{R} + K^2 - K_{mn}K^{mn} - 16\pi\rho \neq 0. \quad (\text{A.4})$$

Here \mathcal{R} is the Ricci scalar of the spatial metric γ_{ij} , K_{ij} is the extrinsic curvature with trace K , and ρ denotes the scalar energy density. Defining the unphysical energy-density contribution

$$\rho_u := \frac{\mathcal{H}_0}{16\pi}, \quad (\text{A.5})$$

Eq. (A.4) can be rewritten as a normal-looking Hamiltonian constraint,

$$\mathcal{H} := \mathcal{R} + K^2 - K_{mn}K^{mn} - 16\pi(\rho + \rho_u) = 0. \quad (\text{A.6})$$

The latter equation shows that our initial data correspond to a total matter-energy density equal to the sum $\rho_{\text{tot}} = \rho + \rho_u$, rather than featuring only the physical energy density ρ . We must therefore *subtract* the effect of the unphysical energy density ρ_u from our ADM-computed initial mass-energy (A.1). We can estimate this unphysical contribution to the ADM mass-energy by integrating ρ_u over the initial hypersurface Σ ,

$$E_u = \int_{\Sigma} \rho_u \sqrt{\gamma} dx^3, \quad \gamma := \det \gamma_{ij}. \quad (\text{A.7})$$

For the BS binary configurations of Table II, a numerical estimation of the integral (A.7) yields²

$$E_u = (1.5 \pm 0.2)V_N, \quad (\text{A.8})$$

and a numerical estimate of the total energy given by

$$E^{\text{NR}} = E_{\text{ADM}}^{\text{NR}}(t=0) - E_u = E_{\text{kin}} - 1.5V_N. \quad (\text{A.9})$$

This result is qualitatively confirmed by computing the ADM integral as a function of time and bearing in mind the constraint damping of the CCZ4 formulation; our code involves (à la Ref. [35]) a constraint damping parameter $\kappa_1 = 0.1/(GM)$. The time evolution $E_{\text{ADM}}^{\text{NR}}(t)$ indeed exhibits an early decrease commensurate with Eq. (A.9), albeit with some numerical noise arising from the discretization error incurred by time evolving the data.

² We obtain the same result by analyzing otherwise identical initial data for binary separations $X/M = 60, 80$ and 100 , indicating the relation's more generic validity.

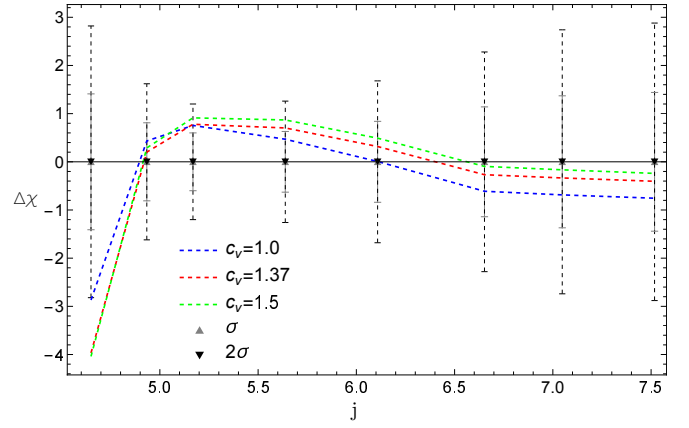


FIG. 4. Difference $\Delta\chi = \chi^{\text{AR}} - \chi^{\text{NR}}$ between the analytic and NR values of the scattering angle for BSBS binaries with initial energy given by Eq. (A.10) with $c_V = 1$, $c_V = 1.37$ and $c_V = 1.5$. The error bars (σ) correspond to the NR results presented in Table I.

Analytic arguments independently validate our expression for the initial energy as follows. We start by assuming that the total incoming energy of the binary can be written as

$$E(c_V) = E_{\text{kin}} + c_V V_N, \quad (\text{A.10})$$

and study the effect of changing the value of the coefficient c_V in front of V_N . From post-Newtonian theory, we know that $c_V = 1 + \mathcal{O}(v^2) + \mathcal{O}(Gm/X)$. For our initial configuration we can neglect $\mathcal{O}(Gm/X)$ compared to $\mathcal{O}(v^2)$. When considering the BH scattering data of Ref. [39] (and evaluating E_{kin} as a function of the incoming momenta), one finds that their $E_{\text{in}}^{\text{NR}}$ is recovered for $c_V \approx 1 + 7v^2$. [The value of c_V depends both on the choice of coordinates, and on the use of a Lagrangian versus an Hamiltonian formalism. For instance, the usual first-order post-Newtonian conserved energy in the Lagrangian approach would feature $c_V = 1 - 7v^2$.] Formally applying the expression $c_V \approx 1 + 7v^2$ to our case (i.e. $v = 0.2291$) yields $c_V \approx 1.37$ in good agreement with Eq. (A.9).

We now show that defining E by Eq. (A.10), with different coefficients c_V , leads to essentially equivalent results for the purpose of our AR/NR comparison of scattering angles. In the main text we compare the scattering data of BSBS binaries to $\chi^{\text{AR}}(E/M, (1+\epsilon_J)J_{\text{NR}}/(GM^2))$ using $E = E(c_V = 1.37)$, and fitting for ϵ_J . The results of the same analysis using $E = E(c_V = 1.0)$ (for which we found $\epsilon_J^{c_V=1.0} = 0.008$) and $E = E(c_V = 1.5)$ (with $\epsilon_J^{c_V=1.5} = 0.005$) are shown in Fig. 4 and Table III. By comparing with Fig. 2 (where $c_V = 1.37$), we see that choosing either $c_V = 1$ or $c_V = 1.37$ or $c_V = 1.5$ has only a minor impact on the scattering angle except for the smallest impact parameter $b = 9.9GM$. Indeed, the differences $\chi^{\text{AR}} - \chi^{\text{NR}}$ measured in units of the NR error bars, namely $\delta_\chi := (\chi^{\text{AR}} - \chi^{\text{NR}})/\Delta\chi^{\text{NR}}$, remain within

TABLE III. Summary of the fractional deviations (δ_χ) of analytic results from numerical results (in units of the NR error bars) for BSBS binaries with the three energy values $E(c_V = 1)$, denoted by $\delta_{\chi,1}$, for $E(c_V = 1.37)$ denoted by $\delta_{\chi,1.37}$, and for $E(c_V = 1.5)$ denoted by $\delta_{\chi,1.5}$.

$b/(GM)$	$\delta_{\chi,1}$	$\delta_{\chi,1.37}$	$\delta_{\chi,1.5}$
9.9	-2.03	-2.81	-2.86
10.5	0.53	0.25	0.36
11.0	1.26	1.30	1.52
12.0	0.74	1.12	1.38
13.0	0.01	0.38	0.58
14.1	-0.54	-0.23	-0.08
15.0	-0.50	-0.24	0.12
16.0	-0.52	-0.28	-0.17

TABLE IV. Summary of the analytically predicted scattering angle along with the deviation from NR results including tidal interactions for BSBS and for BSBS $^{\frac{\pi}{2}}$ (denoted by $\frac{\pi}{2}$) configurations. For all configurations, the total energy is $E_{\text{in}}/M = 1.02394$.

$b/(GM)$	$\chi_{\text{AR}}^{\text{BBH}+w6}$	$\delta_\chi^{\text{BSBS}}$	$\delta_\chi^{\frac{\pi}{2}}$	$\chi_{\text{AR}}^{\text{BBH}+w6+w7}$	$\delta_\chi^{\text{BSBS}}$	$\delta_\chi^{\frac{\pi}{2}}$
9.9	213.55	-2.03	-0.45	214.78	-1.16	0.43
10.5	165.89	0.58	0.75	166.13	0.87	1.04
11.0	143.21	1.49	1.55	143.30	1.64	1.70
12.0	114.93	1.16	1.14	114.95	1.20	1.18
13.0	97.22	0.39	0.78	97.22	0.40	0.79
14.1	83.12	-0.23	-0.19	83.11	-0.23	-0.19
15.0	75.39	-0.24	-0.18	75.39	-0.24	-0.17
16.0	68.03	-0.28	-0.06	68.03	-0.28	-0.06

approximately two standard deviations for all the cases $c_V = 1$, $c_V = 1.37$ and $c_V = 1.5$ (indicated as labels).

Appendix B: Impact of tidal interactions

Here, we illustrate the improvement obtained by including tidal effects for small impact parameter. In order to optimally isolate the tidal effects, we consider the BSBS configurations with minimal scalar interaction. Table IV lists the analytically predicted scattering

angles including the tidal interactions for these configurations; these scattering angles complement the corresponding values reported in the 2nd and 3rd columns of Table II computed *without* tidal effects. While the deviation $\delta_\chi^{\text{BSBS}}$ remains largely unaffected by the inclusion of tidal effects for $b \geq 10.5 GM$, we observe a significant reduction in the deviation from NR results from 3σ to 1σ for the smallest impact parameter $b = 9.9 GM$. This improvement confirms that tidal effects become significant when the two stars get close to each other. A similar comparison for the BSBS $^{\frac{\pi}{2}}$ sequence (cf. the 4th column of Table II) exhibits less improvement after addition of tidal interactions compared to BSBS sequence, probably because the scalar interactions vanish only at leading order for this binary type.

Appendix C: Varying the initial separation

In order to further test the performance of our analytic model, we compare here the AR and NR scattering angles for 5 additional simulations of BSBS binaries with fixed impact parameter $b = 10.5 GM$ but different initial separations. The initial energy is computed from Eq. (A.9) and our results are presented in Table V. The excellent agreement of $\sim 1\sigma$ or better demonstrates the accuracy of our model independent of the initial separation (provided it is large enough to properly define the incoming angle).

TABLE V. Initial separation X , NR scattering angle, analytic scattering for E as given by Eq. (A.10) with $c_V = 1.37$ and deviations δ_χ for the BSBS binary sequences. For all configurations, the impact parameter is $b = 10.5 GM$.

X/M	$\chi_{\text{NR}}^{\text{BSBS}}$	$\chi_{\text{AR}}^{\text{BBH}}$	δ_χ
50.48	165.42(81)	165.62	0.25
60.30	166.08(71)	166.48	0.56
70.12	166.39(58)	167.12	1.26
79.94	166.76(56)	167.62	1.53
89.75	167.09(55)	168.01	1.68
100.27	167.39(55)	168.36	1.76

-
- | | |
|---|---|
| <p>[1] B. P. Abbott <u>et al.</u> (LIGO Scientific, Virgo), Phys. Rev. Lett. 116, 061102 (2016), arXiv:1602.03837 [gr-qc].</p> <p>[2] R. Abbott <u>et al.</u> (KAGRA, VIRGO, LIGO Scientific), Phys. Rev. X 13, 041039 (2023), arXiv:2111.03606 [gr-qc].</p> <p>[3] A. G. Abac <u>et al.</u> (LIGO Scientific, VIRGO, KAGRA), (2025), arXiv:2508.18080 [gr-qc].</p> <p>[4] A. G. Abac <u>et al.</u> (LIGO Scientific, VIRGO, KAGRA), (2025), arXiv:2508.18081 [gr-qc].</p> <p>[5] A. G. Abac <u>et al.</u> (LIGO Scientific, VIRGO, KAGRA), (2025), arXiv:2508.18082 [gr-qc].</p> | <p>[6] R. Abbott <u>et al.</u> (LIGO Scientific, Virgo), Phys. Rev. D 103, 122002 (2021), arXiv:2010.14529 [gr-qc].</p> <p>[7] R. Abbott <u>et al.</u> (LIGO Scientific, VIRGO, KAGRA), Phys. Rev. D 112, 084080 (2025), arXiv:2112.06861 [gr-qc].</p> <p>[8] A. G. Abac <u>et al.</u> (LIGO Scientific, Virgo, KAGRA), Phys. Rev. Lett. 135, 111403 (2025), arXiv:2509.08054 [gr-qc].</p> <p>[9] B. P. Abbott <u>et al.</u> (LIGO Scientific, Virgo), Phys. Rev. Lett. 119, 161101 (2017), arXiv:1710.05832 [gr-qc].</p> |
|---|---|

- [10] A. G. Abac et al. (LIGO Scientific, VIRGO, KAGRA), (2025), arXiv:2507.08219 [astro-ph.HE].
- [11] J. C. Aurrekoetxea, C. Hoy, and M. Hannam, Phys. Rev. Lett. **132**, 181401 (2024), arXiv:2312.03860 [gr-qc].
- [12] J. Calderón Bustillo, N. Sanchis-Gual, A. Torres-Forné, J. A. Font, A. Vajpeyi, R. Smith, C. Herdeiro, E. Radu, and S. H. W. Leong, Phys. Rev. Lett. **126**, 081101 (2021), arXiv:2009.05376 [gr-qc].
- [13] S. Clesse and J. Garcia-Bellido, Phys. Dark Univ. **38**, 101111 (2022), arXiv:2007.06481 [astro-ph.CO].
- [14] T. Evstafyeva, U. Sperhake, I. Romero-Shaw, and M. Agathos, Phys. Rev. Lett. **133**, 131401 (2024), arXiv:2406.02715 [gr-qc], arXiv:2406.02715 [gr-qc].
- [15] S. L. Liebling and C. Palenzuela, Living Rev. Rel. **26**, 1 (2023), arXiv:1202.5809 [gr-qc].
- [16] H. Kim, J. Park, and M. Son, JHEP **07**, 150 (2024), arXiv:2402.00741 [hep-ph].
- [17] T. Vachaspati and A. Vilenkin, Phys. Rev. Lett. **67**, 1057 (1991).
- [18] D. Inman and Y. Ali-Haïmoud, Phys. Rev. D **100**, 083528 (2019), arXiv:1907.08129 [astro-ph.CO].
- [19] P. V. P. Cunha, C. Herdeiro, E. Radu, and N. Sanchis-Gual, Phys. Rev. Lett. **130**, 061401 (2023), arXiv:2207.13713 [gr-qc].
- [20] N. Siemonsen, Phys. Rev. Lett. **133**, 031401 (2024), arXiv:2404.14536 [gr-qc].
- [21] G. A. Marks, S. J. Staelens, T. Evstafyeva, and U. Sperhake, (2025), arXiv:2504.17775 [gr-qc].
- [22] T. Evstafyeva, N. Siemonsen, and W. E. East, (2025), arXiv:2508.11527 [gr-qc].
- [23] M. W. Choptuik and F. Pretorius, Phys. Rev. Lett. **104**, 111101 (2010), arXiv:0908.1780 [gr-qc].
- [24] A. Gonzalez, S. Bernuzzi, A. Rashti, F. Brandoli, and R. Gamba, (2025), arXiv:2507.00113 [gr-qc].
- [25] C. Palenzuela, P. Pani, M. Bezares, V. Cardoso, L. Lehner, and S. Liebling, Phys. Rev. D **96**, 104058 (2017), arXiv:1710.09432 [gr-qc].
- [26] R. Brito, V. Cardoso, C. A. R. Herdeiro, and E. Radu, Phys. Lett. **B752**, 291 (2016), arXiv:1508.05395 [gr-qc].
- [27] M. Alcubierre, J. Barranco, A. Bernal, J. C. Degollado, A. Diez-Tejedor, M. Megevand, D. Nunez, and O. Sarbach, Class. Quant. Grav. **35**, 19LT01 (2018), arXiv:1805.11488 [gr-qc].
- [28] D. J. Kaup, PR **172**, 1331 (1968).
- [29] R. Ruffini and S. Bonazzola, Phys. Rev. **187**, 1767 (1969).
- [30] L. Visinelli, (2021), arXiv:2109.05481 [gr-qc].
- [31] A. Buonanno and T. Damour, Phys. Rev. D **59**, 084006 (1999), gr-qc/9811091.
- [32] S. Carloni and J. a. L. Rosa, Phys. Rev. D **100**, 025014 (2019), arXiv:1906.00702 [gr-qc].
- [33] U. Sperhake, Phys. Rev. D **76**, 104015 (2007), gr-qc/0606079.
- [34] G. Allen, T. Goodale, J. Massó, and E. Seidel, “The cactus computational toolkit and using distributed computing to collide neutron stars,” (1999), presented at the Eighth IEEE International Symposium on High Performance Distributed Computing (HPDC-8), Redondo Beach, California, 1999.
- [35] D. Alic, C. Bona-Casas, C. Bona, L. Rezzolla, and C. Palenzuela, Phys. Rev. D **85**, 064040 (2012), arXiv:1106.2254 [gr-qc].
- [36] E. Schnetter, S. H. Hawley, and I. Hawke, Class. Quant. Grav. **21**, 1465 (2004), gr-qc/0310042.
- [37] T. Helfer, U. Sperhake, R. Croft, M. Radia, B.-X. Ge, and E. A. Lim, Class. Quant. Grav. **39**, 074001 (2022), arXiv:2108.11995 [gr-qc].
- [38] E.ourgoulhon, (2007), arXiv:gr-qc/0703035.
- [39] T. Damour, F. Guercilena, I. Hinder, S. Hopper, A. Nagar, and L. Rezzolla, Phys. Rev. D **89**, 081503 (2014), arXiv:1402.7307 [gr-qc].
- [40] S. Hopper, A. Nagar, and P. Retegno, Phys. Rev. D **107**, 124034 (2023), arXiv:2204.10299 [gr-qc].
- [41] T. Damour and P. Retegno, Phys. Rev. D **107**, 064051 (2023), arXiv:2211.01399 [gr-qc].
- [42] P. Retegno, G. Pratten, L. M. Thomas, P. Schmidt, and T. Damour, Phys. Rev. D **108**, 124016 (2023), arXiv:2307.06999 [gr-qc].
- [43] S. Swain, G. Pratten, and P. Schmidt, (2024), arXiv:2411.09652 [gr-qc].
- [44] A. Buonanno, G. U. Jakobsen, and G. Mogull, Phys. Rev. D **110**, 044038 (2024), arXiv:2402.12342 [gr-qc].
- [45] O. Long, H. P. Pfeiffer, A. Buonanno, G. U. Jakobsen, G. Mogull, A. Ramos-Buades, H. R. Rüter, L. E. Kidder, and M. A. Scheel, (2025), arXiv:2507.08071 [gr-qc].
- [46] T. Damour, Phys. Rev. D **97**, 044038 (2018), arXiv:1710.10599 [gr-qc].
- [47] G. Kälin, Z. Liu, and R. A. Porto, Phys. Rev. D **102**, 124025 (2020), arXiv:2008.06047 [hep-th].
- [48] D. Bini, T. Damour, and A. Geralico, Phys. Rev. D **104**, 084031 (2021), arXiv:2107.08896 [gr-qc].
- [49] D. Bini, T. Damour, and A. Geralico, Phys. Rev. D **101**, 044039 (2020), arXiv:2001.00352 [gr-qc].
- [50] C. Cheung and M. P. Solon, Phys. Rev. Lett. **125**, 191601 (2020), arXiv:2006.06665 [hep-th].
- [51] C. Palenzuela, I. Olabarrieta, L. Lehner, and S. L. Liebling, Phys. Rev. D **75**, 064005 (2007), gr-qc/0612067.
- [52] N. Sennett, T. Hinderer, J. Steinhoff, A. Buonanno, and S. Ossokine, Phys. Rev. D **96**, 024002 (2017), arXiv:1704.08651 [gr-qc].
- [53] T. Damour and N. Deruelle, Annales de L’Institut Henri Poincaré Section (A) Physique Theorique **44**, 263 (1986).